Journal of Materials Chemistry A

Hierarchical Chemomechanical Encoding of Multi-Responsive Hydrogel Actuators via 3D Printing

Journal:	*Journal of Materials Chemistry A*
Manuscript ID	TA-ART-04-2019-003547.R1
Article Type:	Paper
Date Submitted by the Author:	23-May-2019
Complete List of Authors:	ODENT, JEREMY; Universite de Mons, Laboratory of Polymeric and Composite Materials (LPCM) Vanderstappen, Sophie; Universite de Mons, Laboratory of Polymeric and Composite Materials (LPCM) Toncheva, Antoniya; Universite de Mons, Pichon, Enzo; Universite de Mons, Laboratory of Polymeric and Composite Materials (LPCM) Wallin, Thomas; Cornell University, Materials Science and Engineering Wang, Kaiyang; Cornell University, b. Sibley School of Mechanical and Aerospace Engineering Shepherd, Robert; Cornell University, Mechanical & Aerospace Engineering Dubois, Philippe; Universite de Mons, Raquez, Jean-Marie; University of Mons - UMONS, Laboratory of Polymeric and Composite Materials (LPCM)

ARTICLE

Hierarchical Chemomechanical Encoding of Multi-Responsive Hydrogel Actuators via 3D Printing

Received 00th January 20xx,
Accepted 00th January 20xx

DOI: 10.1039/x0xx00000x

Jérémy Odent,*[a] Sophie Vanderstappen,[a] Antoniya Toncheva,[a,b] Enzo Pichon,[a] Thomas J. Wallin,[c,d] Kaiyang Wang,[c] Robert F. Shepherd,[c] Philippe Dubois[a] and Jean-Marie Raquez*[a]

Inspired by nature, we herein demonstrate a family of multi-responsive hydrogel-based actuators that are encoded with anisotropic swelling behavior to provide rapid and controllable motion. Fabrication of the proposed anisotropy-encoded hydrogel actuators relies on the high resolution stereolithography 3D printing of functionally graded structures made of discrete layers having different volume expansion properties. Three separate synthetic strategies based on *i)* an asymmetrical distribution of layer's surface area to volume ratio via mechanical design, *ii)* crosslinking density via UV photo-exposure, or *iii)* chemical composition via resin vat exchange have been accordingly demonstrated for developing such smooth gradients within the printed hydrogel-based actuator. Our chemomechanical programming enable fast, reversible, repeatable and multimodal bending actuation in response to any immediate environmental change (*i.e.* based on osmotic pressure, temperature and pH) from a single printed structure.

Introduction

Active motion is ubiquitous in nature, where a multitude of complex movements mainly relies on the tissue composition and microstructural anisotropy of cells[1, 2]. The latter is exemplified by nastic plant motions, driven by the difference in local swelling behavior that arise from the specific directional orientation of cellulose fibrils within plant cells[3, 4]. Mimicking biological designs in man-made structures is naturally recognized as sources of scientific and technological inspiration for the development of unique bio-inspired actuators and self-deployable devices with conferred functionality[5]. Undergoing controllable motion offers exciting expectations for a wide range of applications including space exploration[6], biomedical devices[7] and soft robotics[8]. Different emerging pathways have been constructed around the development of *e.g.* shape-memory polymers[9, 10], hydrogels[2, 11] or (nano)composites[12, 13].

Hydrogels, *i.e.* three-dimensional polymer networks imbibed with aqueous solutions, can reversibly change their volume or shapes upon the trigger of environmental stimuli such as temperature, pH, and ionic strength[14-16]. Since hydrogels usually have isotropic structures (*i.e.* structural and compositional uniformity in all directions), they normally provide homogeneous expansion or contraction in all directions[17]. An anisotropy, *i.e.* inhomogeneity with different magnitudes towards any direction is therefore required to generate complex deformation such as bending and twisting. Such anisotropy could be achieved either by applying a gradient of stimuli (*e.g.* temperature, pH, light, among others) to homogeneous materials or a non-gradient stimuli to inhomogeneous materials (*e.g.* gradient-like structures)[18, 19]. While the former is technically complicated to implement as a continuous gradient of stimuli must be formed and maintained for a long period of time, the latter can lead to more complex deformations (*i.e.* formation of hinges, bidirectional bending, *etc.*) due to the difference in properties between the constituting components. Early examples included the fabrication of differential crosslinking density[20, 21] and the generation of smooth gradients in composition[22, 23] or nanoparticles[24, 25] within the materials. Among them, designing bilayer structures containing one passive structural layer and another active layer is an efficient way to confer anisotropy[26-30]. Although considerable progress has been achieved to drive programmed changes in structure, most approaches have been heavily restricted to conventional fabricating methods that are inherently limited to the simple two-dimensional (2D) construction.

Accessing a method for novel shape generation that provides three-dimensional (3D) deformation is highly demanded. Advanced additive manufacturing technologies, also known as 3D printing techniques, has been herein recognized as the milestone technology for the fabrication of complex objects with unusual geometries[31, 32]. Slowly yet steadily, direct 3D printing of active structures gave birth to a brand new 4D printing technology with an outlined time

[a] Laboratory of Polymeric and Composite Materials (LPCM), Center of Innovation and Research in Materials and Polymers (CIRMAP), University of Mons (UMONS), Place du Parc 20, 7000 Mons, Belgium.
[b] Laboratory of Bioactive polymers, Institute of Polymers, Bulgarian academy of sciences, Akad. G. Bonchev St. 103A, 1113 Sofia, Bulgaria.
[c] Sibley School of Mechanical and Aerospace Engineering, Cornell University, Ithaca, NY 14853, USA.
[d] Facebook Reality Labs, Redmond, Washington, USA.
† Electronic Supplementary Information (ESI) available.
See DOI: 10.1039/x0xx00000x

dimension, allowing the as-printed object to change its form or function with time in response to stimuli[33, 34]. As such, the review by Miao *et al.*[35] provide extensive summary of state-of-art technological advances in the field of 4D printing. For example, 3D-printed structures made of two different water-absorbing materials came into light with the concept of 4D printing where the water-stimulated volume difference caused the fabricated structure to bend[36, 37]. Recently, direct ink writing (DIW) of composite-gels permitted alignment cellulose fibrils in response to the imposed shear during printing[1] ; the resulting anisotropy in Young's modulus yields programmed actuation. This strategy, though, is only compatible with composites possessing high aspect ratio particles and endemic issues with DIW (*i.e.* a trade-off in print resolution and speed, difficulty to directly fabricating overhanging features) persist[42]. Stereolithography (SLA), by comparison, uses the spatial-temporal resolution of light to photopolymerize objects from a liquid resin. There is no loss in print speed or resolution when scaling the photopattern and the buoyant support provided by printing within a vat of liquid resin enables high aspect ratio soft features to be directly printed[42]. Yet, computer-aided design tools are not set up to generate such desired structural gradients, lacking the possibility of controlling the material's directional dependence in the generation of form[38, 39]. In light of these limitations, a breakthrough strategy towards designing SLA-printed gradient-like structures, *i.e.* a layered structure where the density of the structure change stepwise along one axis, is reported. The core technology of this research varies from others in that controlling the anisotropic swelling property by means of tuning swelling rates, crosslinking density and chemical composition of discrete layers can precisely predetermine the folding of the multilayered structures. Given the significance of controlling the material anisotropy, gradient-like structures may provide new insights to design and fabricate multi-responsive actuators[40, 41].

Here, the high resolution SLA 3D printing allow to design a family of multi-responsive hydrogel-based actuators with rapid, reversible and repeatable self-bending characteristics using a simple and versatile platform. In this approach, a special attention was paid to the material design in order to generate structural anisotropy within the final object, thereby assuring triggered and remote control of the material's transformation. This work represents a flexible platform for designing more advanced actuators beyond the present study that would enrich the fields of smart materials and promote new potential applications.

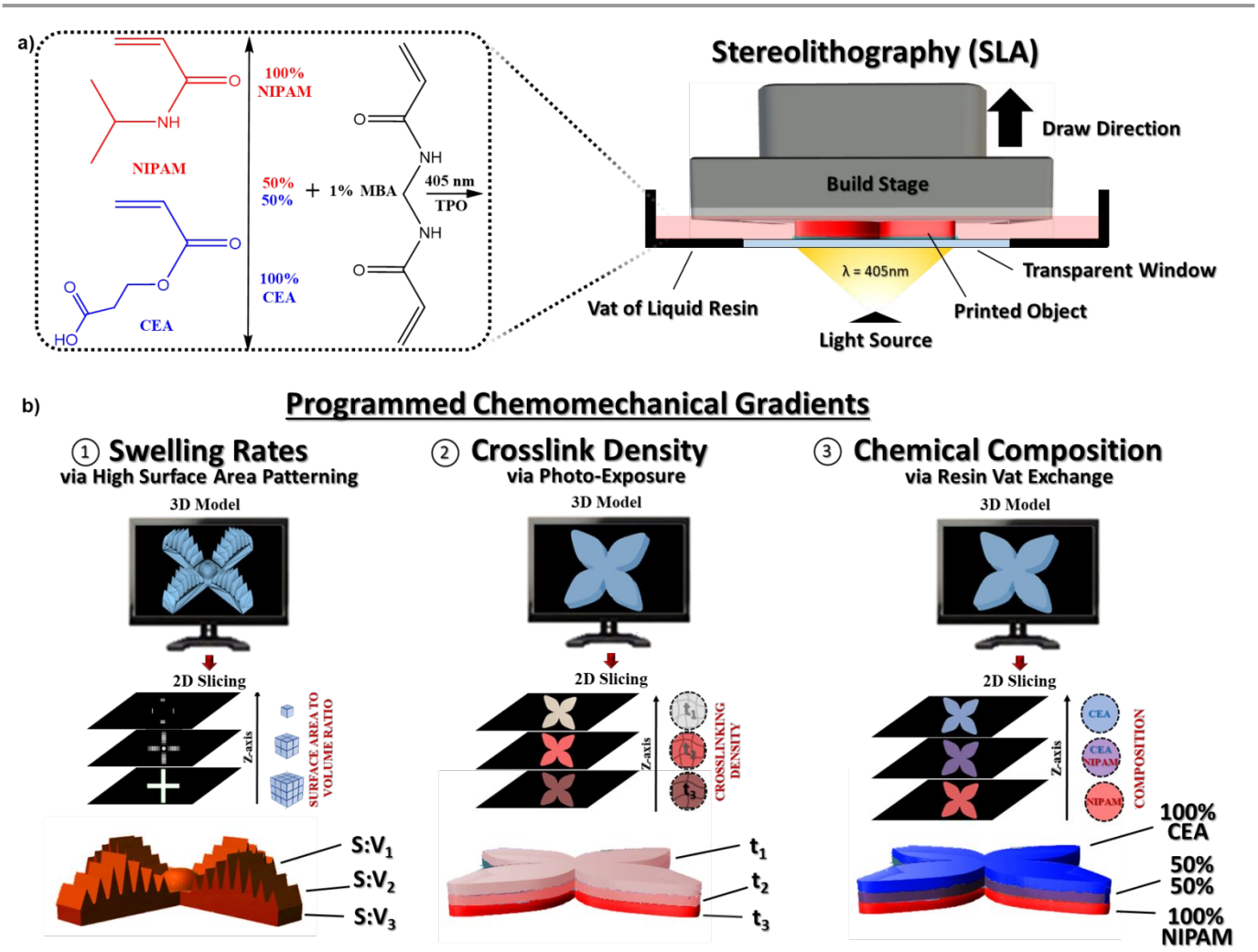

Figure 1. General strategy towards designing 3D-printed gradient-like structures. (A) Chemistry and fast bottom-up fabrication of gradient-like structures via photo-polymerization of NIPAM and CEA using TPO photo-initiator and MBA crosslinker. **(B)** Three separate synthetic gradient-like structures by means of varying *i)* the specific surface area to volume ratio from computer 3D models, *ii)* the crosslinking density via near-UV exposure time and *iii)* the chemical composition via resin vat exchange of discrete layers during the 3D printing process.

Results and Discussion

Design and 3D printing of gradient-like structures. In the present study, we propose a general approach for the design of stimuli-responsive hydrogel-based materials that are encoded with anisotropic swelling behavior to provide rapid and controllable motion. As a model system, *N*-isopropylacrylamide, NIPAM, and 2-carboxyethylacrylate, CEA, commonly combined with small amounts of *N,N'*-methylenebisacrylamide, MBA, as crosslinker, are used to form the proposed hydrogels. Fabrication of such hydrogels into complex geometries with high-resolution features is based on an Ember™ (Autodesk, Inc.) digital mask projection SLA printer, where the photo-pattern is projected through a transparent, oxygen permeable window at the base of a vat of liquid resin. Diphenyl(2,4,6-trimethylbenzoyl)phosphine oxide), TPO, a type-I photo-initiator, enables free radical photo-polymerization of the acrylate groups within near-UV exposure. Photo-rheology allows the *in-situ* monitoring of chemical and mechanical characteristics during the photo-polymerization reaction. A three orders of magnitude increase in complex viscosity within *ca.* 7s of illumination (Irradiant flux, H_e = 140 mJ · cm^2 and wavelength, λ = 405 nm) represents the key-feature for the rapid fabrication of macro-scale objects using commercial SLA technology (Figure S1 in the SI). This processing window enabled us to design 3D-printed objects with actuation performances upon the nature of the acrylic monomers.

Among them, poly(*N*-isopropylacrylamide), PNIPAM, and poly(2-carboxyethylacrylate), PCEA, are selected as polymeric partners whose solubility, volume and chain conformation can be manipulated by changes in temperatures and pH with respect to its lower critical solution temperature (LCST, *ca.* 32°C for PNIPAM) and its acid dissociation constant (pKa, *ca.* 5.8 for PCEA). These conditions typically result in expansion/contraction of the whole material volume caused by homogeneous swelling/shrinkage of the hydrogel in all directions. Expected bending/unbending movements are typically the result of inhomogeneous swelling, which occurs at different magnitude upon different direction. Strategies to develop stimuli-responsive hydrogels that are able to bend/unbend in response to environmental stimuli herein rely on the fabrication of an asymmetrical distribution in material properties, composition or microstructure across the hydrogel. The latter requires the absolute spatial control over material placement and structure creation over the entire 3D printing process. SLA thereby represents the primary technological focus of this work as it provides an easy access to each individual building layers during fabrication[43, 44]. Herein, anisotropy-encoded hydrogel actuators are expected from the generation of gradient-like structures where each individual building layers own different volume expansion properties. As the swelling of any polymer network depends upon *i)* the dimension of the as-obtained gel, *ii)* the degree of crosslinking and *iii)* the nature of the polymer, controlling either *i)* the specific surface area to volume ratio, *ii)* the crosslinking density or *iii)* the chemical composition of discrete layers during fabrication should provide opportunities to confer anisotropy within the final object (Figure 1 and Figure S2 in the SI). Further, the strategies outlined herein are not mutually exclusive, a single printed object can employ any combination thereof to encode the desired anisotropies. Though, three distinct methods for programming in chemomechanical gradients on bending actuation are herein demonstrated and discussed in the following subsections.

Surface area to volume ratio. The dimension (size, shape, *etc.*) of the final hydrogel is of prime importance on the swelling kinetics. Changing the surface area-to-volume (S:V) ratio across the hydrogel can thereby represent a simple and efficient pathway to construct anisotropy-encoded hydrogel actuators. These actuators hold the promise to generate substantial forces while only consuming modest amounts of energy[45]. In light of these features, we aimed to develop centimeter-scaled osmotically-driven actuators that are capable of generating suitable forces to provide rapid and controllable motion. The latter requires the absolute spatial control over the dimensional feature of the desired object from computer models, leading to a layered structure of varying S:V ratio along the printing Z-axis (see Figure 2a and Figure S2 in the SI). In line of the theory of the swelling kinetics of gels presented by Tanaka *et al.*[46], the characteristic time of swelling is proportional to the square of a linear dimension of the gel and its diffusion coefficient.

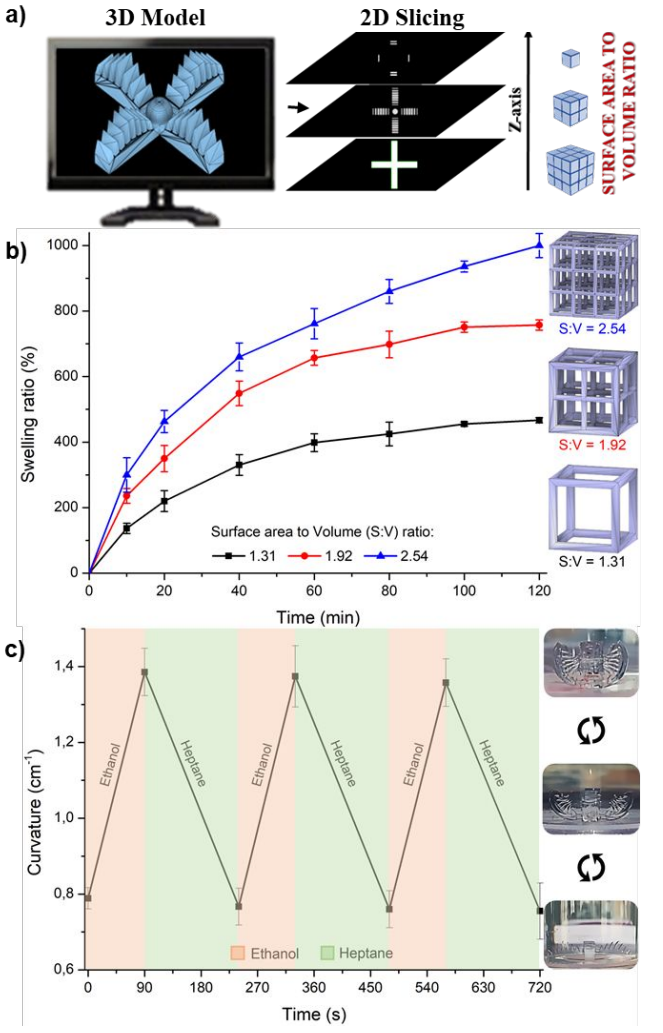

Figure 2. Performances of gradient-like PNIPAM structures of varying surface area to volume ratio. (A) Fabrication of gradient-like structures by means of varying the specific surface area to volume ratio of discrete layers along the printing Z-axis. **(B)** Swelling performance of 3D-printed PNIPAM cubic lattices with different S:V ratio in ethanol. **(C)** Cyclic reversible osmotically-driven actuation of 3D-printed PNIPAM gradient-like structures of varying S:V ratio (the distribution of the calculated S:V ratio into the multi-armed gripper is shown in Figure S2).

We accordingly used our ability to photo-pattern 3D structures to print cubic lattices (dimensions: 2 cm³) of similar network diffusion coefficients (using the same material, *i.e.* PNIPAM, and printing process, *i.e.* illumination per layer of 3s per 100 µm to provide an estimated crosslink density of $1*10^{-6}$ mol/cm³) but of varying S:V ratio for rapid osmotic actuation. The higher the S:V ratio of the structure, the greater the swelling ratio at larger time scales (Figure 2b). The Power-Law fits of the data and the value diffusion exponents (n ☐ 0.5) suggest simple Fickian diffusion (Figure S3a in the SI). Swelling *vs.* the square root of immersion time was further plotted, while dividing the as-determined slope-values by the corresponding S:V ratios allows us to confirm the observation that the swelling rate scales linearly with the S:V ratio (Figure S3 in the SI). Unlike conventional fabricated smart-gels, where the device is miniaturized to enhance S:V ratio, the ability to pattern high surface area features permits rapid swelling in larger objects (on the order of cms). Such as-designed objects are then able to achieve greater osmotic pressure through the solvent-hydrogel boundary without constraining the overall size of the device. This strategy permits direction actuation without altering the mechanics of the underlying material (*i.e.* Young's Modulus, ultimate strain, *etc.*). This process is also reversible once the hydrogels are placed in an unfavorable environment (*i.e.* a non-solvent such as heptane) (Figure S4 in the SI).

To demonstrate our control over diffusive swelling, we 3D-printed PNIPAM multi-armed grippers (dimensions: 2 cm length, 0.4 cm thickness) consisting of a gradient-like structure where the S:V ratio of discrete layers change stepwise along the printing Z-axis. The high surface area patterning thereby accommodate the swelling locally which determine the bending motion (see Figure S2 in the SI). Once immerged in ethanol from an initial dry state, the resulting object is able to reversibly and repeatedly swell from an initially flat and open state to curved and enclosed within minutes. That is, the centimeter scaled multi-armed gripper deform rapidly, resulting in a bending curvature of *ca.* 1.4 cm^{-1} in 90s and leading to one complete reversible cycle in about 240s (Figure S5 in the SI). As curvature of bending scales inversely with the dimensions of the device, existing osmotically-driven actuators generally suffer from the intrinsic coupling between responsive times and the actuation forces[47, 48]. As-printed gradient-like structures of varying S:V ratio then allow for the simultaneous combination of fast actuation and large-scale deformation that existing osmotic hydrogel actuators do not exhibit yet in terms of the response rate and the amplitude of movement with respect to its dimension. In addition, the osmotically-driven actuators can maintain robustness and functionality over multiple cycles of actuation without obvious performance-loss or failure, supporting the anti-fatigue behavior of the resulting 3D-printed gradient-like structures under moderate stresses (Figure 2c).

Crosslinking density. The degree of crosslinking is herein assumed as another swelling differentiator. The simple control over the near-UV exposure time of discrete layers during the 3D printing process, with respect to their respective crosslinking density, is thereby envisioned as an alternative towards designing anisotropy-encoded hydrogel actuators. Obviously, PNIPAM hydrogels of similar dimensions (*i.e.* using flat and dense 3D models) but of varying crosslinking density were fabricated to avoid any undesired contribution of the dimensionality to the swelling behavior. Herein, the ability of PNIPAM to undergo an entropy-driven phase transition from a soluble to an insoluble aggregated state above its LCST offers a convenient and tunable method to control their physicochemical properties with respect to any immediate environmental change[49]. That is, the subsequent release of entrapped water molecules from the swollen PNIPAM hydrogel network once placed above the LCST (*ca.* 32°C) result on a significant volume reduction.

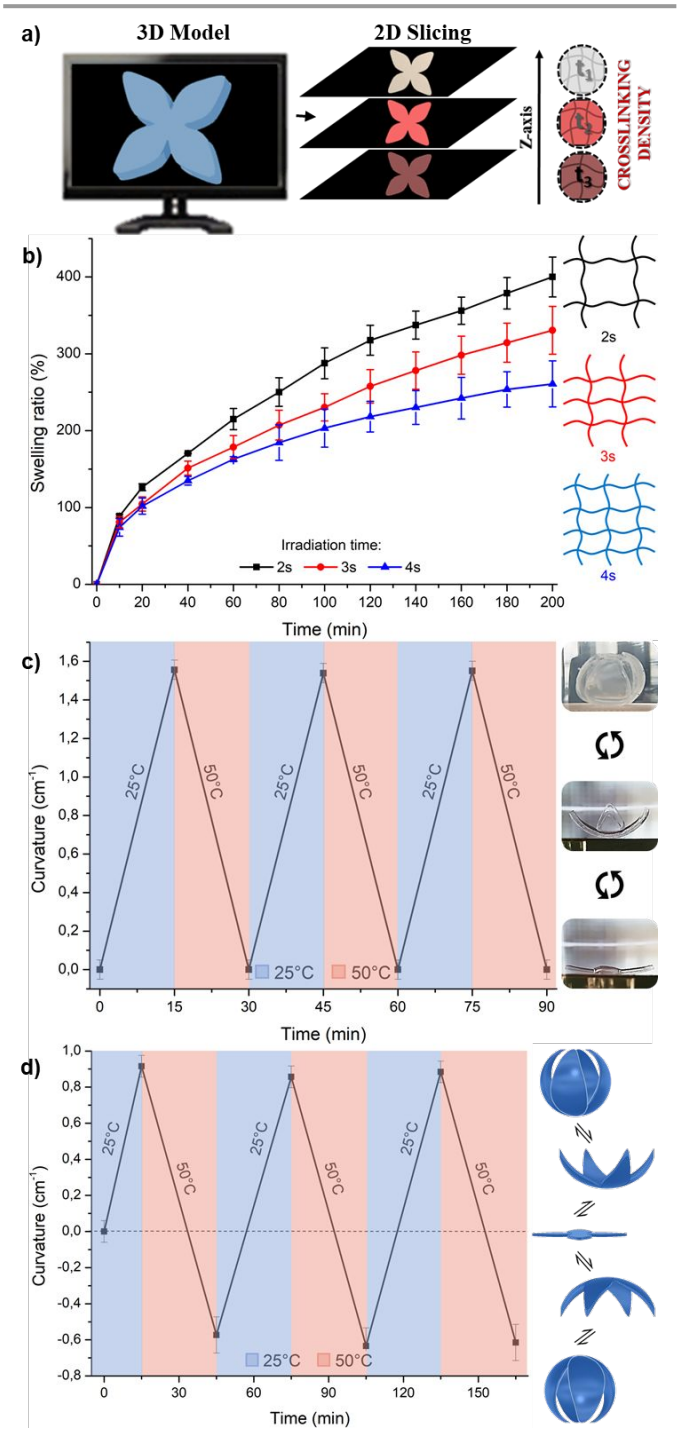

Figure 3. Performances of gradient-like PNIPAM structures of varying crosslinking density. (A) Fabrication of gradient-like structures by means of varying the crosslinking density of discrete layers along the printing Z-axis. **(B)** Swelling performance of 3D-printed PNIPAM-based hydrogels with different crosslinking density by means of controlling the near-UV exposure time. **(C)** Cyclic reversible thermally-driven monodirectional and **(D)** bidirectional actuation of 3D-printed gradient-like structures of varying crosslinking density across the hydrogel (the lowest crosslinking density is at the bottom of the structure).

Thanks to the aforementioned unique properties, we herein aimed to develop temperature-controlled manipulators by fabricating an asymmetrical distribution of crosslinking density across the PNIPAM hydrogel. Such structural inhomogeneity can be generated by varying the near-UV exposure time along the printing Z-axis (see Figure 3a and Figure S2 in the SI). It is important to note that the cumulative photoirradiation dose may be the sum of numerous exposures, particularly for transparent resins as light can penetrate multiple successive Z-layers. Note also that hydroquinone is further included in the formulation as a radical scavenger to avoid any undesired diffusional curing beyond the built layer, which improve the resolution of large-scale prints and pot-life of the resins.

The correlation between the near-UV light photo-exposure and hydrogel properties is particularly elucidated by rheological investigations on printed disks (dimensions: 2 cm length, 0.1 cm thickness) (Figure S6 in the SI). Oscillation amplitude sweeps of the hydrogels of varying crosslinking density thereby attested a typical elastic solid behavior, that is, the storage modulus (G') is higher than the loss modulus (G"). As expected, raising the near-UV exposure time significantly increases the hydrogel stiffness as evidenced by higher values for both G' and G". An estimation of the effective crosslinking density is further attempted by modulus measurements in the rubbery plateau, assuming a linear relationship between exposure time and crosslinking density (Figure S6 in the SI). That is, the relationship between rubbery plateau and crosslink density is given by $\upsilon_e = G'/RT$ where υ_e is the crosslink density, G' is the shear modulus obtained in the rubbery plateau, T is the temperature and R is the gas constant[50]. An estimated crosslink density of $0.4*10^{-6}$, $1*10^{-6}$ and $1.8*10^{-6}$ mol/cm³, respectively at 2s, 3s and 4s of UV photo-exposure are thereby determined by use of this equation. Besides, resulting hydrogels of different crosslinking density but of similar chemical composition and surface area to volume ratio demonstrated different swelling behavior (Figure 3b and Figure S7 in the SI). Recall that the dimension (size, shape, *etc.*) of the final hydrogel is of prime importance on the swelling kinetics, we should notice that 3D-printed PNIPAM hydrogels in cylindrical shaped (dimensions: 6 mm length, 3 mm thickness) were used to characterize the swelling performance reported here. It came out that the higher the crosslinking density, the smaller the swelling ratio at larger time scales. The kinetics of swelling of these hydrogels are further categorized as Fickian from the Power-Law fits of the data (diffusion exponents n ☐ 0.5) and the linear behavior against the square root of immersion time (Figure S8 in the SI). As expected, raising the near-UV exposure time (*i.e.* the crosslink density of the 3D-printed PNIPAM hydrogels) lead to lower swelling performance as evidenced by a swelling ratio of 108%, 94% and 86% within 15 min in water, respectively at 2s, 3s and 4s of near-UV exposure (Figure 3b). Such a difference in the swelling performance is high enough to generate suitable forces to provide rapid and controllable motion.

We thereby exploited the thermo-induced volume change of PNIPAM hydrogels of differential crosslinking density to driven actuation. That is, the 3D-printed PNIPAM flower-like multi-armed grippers (dimensions: 2 cm length, 0.18 cm thickness) is able to reversibly and repeatedly bend up to *ca.* 1.55 cm^{-1} in 15 min (starting from the dry state) upon thermal stimulation (25°C *vs.* 50°C) in water (Figure 3c and Figure S9 in the SI). The motion typically results from the inhomogeneous swelling of discrete layers that compose the functionally graded PNIPAM hydrogel (into water at 25°C). This process is also reversible once the anisotropic PNIPAM hydrogels are placed in hot water (*i.e.* above the LCST), releasing entrapped water molecules from the swollen PNIPAM hydrogel network and leading to the volume reduction. Surprisingly, the proposed gradient-like hydrogel actuator of varying crosslinking density revealed continuous bidirectional bending in response to temperature (bend from -0.6 cm^{-1} to 0.9 cm^{-1} in 30 min in water

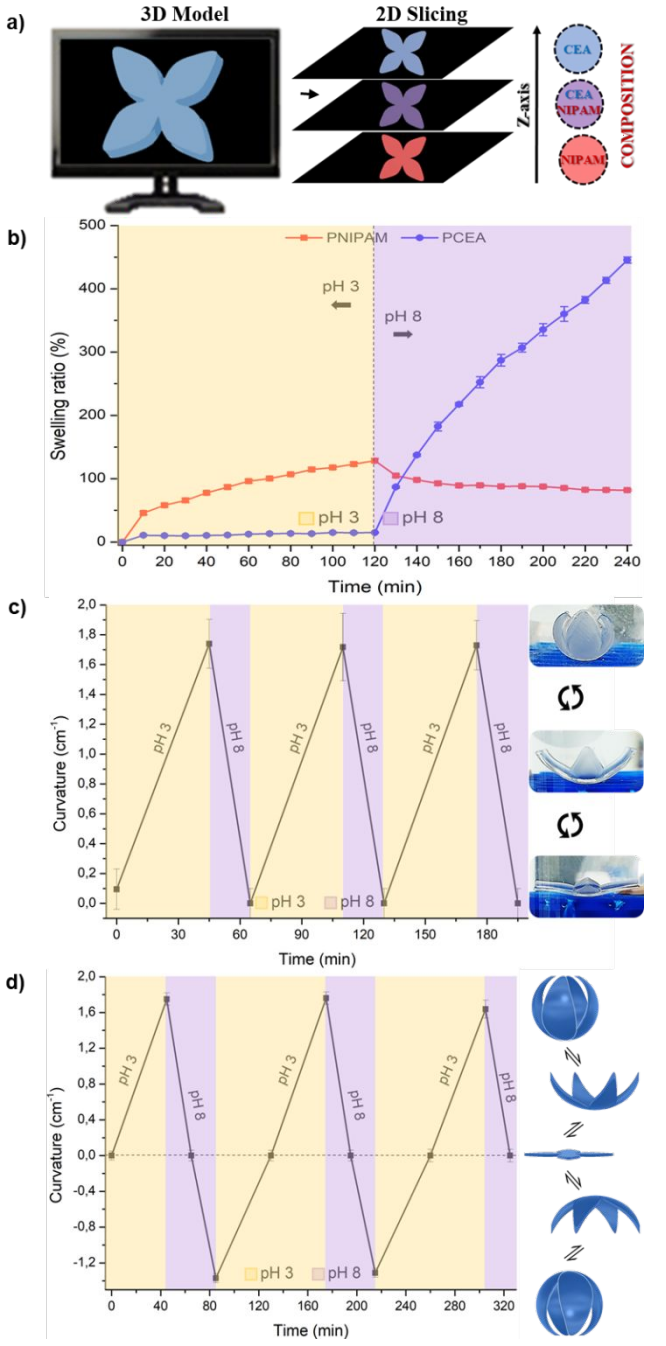

Figure 4. Performances of gradient-like structures of varying composition. (A) Fabrication of gradient-like structures by means of varying the chemical composition of discrete layers from PNIPAM to PCEA along the printing Z-axis. **(B)** Swelling performance of 3D-printed gradient-like structures of varying layer's composition across the hydrogel. **(C)** Cyclic reversible pH-driven monodirectional and **(D)** bidirectional actuation of 3D-printed gradient-like structures of varying layer's composition across the hydrogel (PNIPAM is at the bottom of the structure).

at 25°C and back to -0.6 cm^{-1} in 30 min in water at 50°C) that existing thermally driven actuators do not exhibit yet as they are generally limited to one directional bending[26] (Figure 3d). Likely, the bidirectional bending property results from the unequal forces generated by asynchronous temperature-triggered swelling and shrinkage of hydrogel layers with different crosslinking density.

Composition. To further confirm the synthetic flexibility that can be achieved using SLA, we purposely designed layered structures consisting of passive and active layers towards pH-type stimulus. Fabrication of the proposed anisotropy-encoded design comes from the gradual compositional distribution of thermo-responsive PNIPAM and pH-responsive PCEA across hydrogels of similar dimensions and crosslinking density (*i.e.* using flat and dense 3D models and an illumination per layer of 3s per 100 µm as characterized by an estimated crosslink density of $1*10^{-6}$ mol/cm^3) (Figure 4a and Figure S2 in the SI). Such multiple materials can be managed during the 3D printing process by simply exchanging the formulation within the vat. Probing the individual sensitivity of discrete PNIPAM and PCEA layers towards pH-type stimulus herein provide new insights into designing fast responsive anisotropy-encoded actuators (Figure 4b). It turns out that PCEA swells at high pH values, consistent with the deprotonation of the carboxylic acid in an alkaline environment. Specifically, carboxylic acids are substantially protonated at pH 3, though, its ionization occurred when placed at pH 8 (above its pKa value, *ca.* 5.8 for PCEA), resulting in electrostatic repulsion between the polymer network that contribute to higher water absorption and volume expansion[51]. In contrast, PNIPAM does not respond as effectively to pH changes. PNIPAM will only slightly swell within strong acidic/basic solutions, disrupting the weaker secondary hydrogen bonds between PNIPAM molecules[52].

Harnessing the pH-responsive volume-change of respective discrete layers is thereby envisioned as an efficient pathway to confer desired bending actions. That is, the 3D-printed macro-scale object consist of a structural PNIPAM-based layer and another pH-responsive PCEA-based layer, bonded together by an intermediate P[NIPAM-*co*-CEA] (50/50 mol%) layer at the interface. Resin-replacement enables compositional changes between build layers and the shared acrylate moieties on the monomers permits covalent bonds to form between materials. In line of the asymmetrical distribution of layer's chemical composition across the hydrogel, reversible and repeatable bending actuation have been constructed (Figure 4c). The driving force for initiating the bending actuation is mainly attributed to the residual internal stress programmed in discrete layers with specific swelling properties. The aforementioned unique properties led the macro-scale object to bend one complete reversible cycle in about 65 min upon pH stimulation (Figure S10 in the SI). That is, the as-printed flower-like multi-armed grippers (dimensions: 2 cm length, 0.18 cm thickness) bend up to *ca.* 1.75 cm^{-1} in 45 min at pH 3 (starting from the dry state) and reverses in 20 min at pH 8. Note that patterning an actuator with a higher S:V ratio would improve these cycle times. Bidirectional bending property in response to pH is once again reached (bend from -1.4 cm^{-1} to 1.7 cm^{-1} in 90 min at pH3 and back to -1.4 cm^{-1} in 45 min at pH8) thanks to the differential swellability of discrete layers within the generated actuator (Figure 4d). Apart from the pH stimulus, such manipulators are temperature-sensitive as well with respect to its PNIPAM composition, providing temperature and pH dual-responsive hydrogels. When the pH is maintained and temperature is increased to 50°C (*i.e.* above the LCST of PNIPAM), the hydrogel actuator bend further toward the PNIPAM layer with respect to its thermo-induced volume contraction (Figure 5a). The bending states of the resulting gradient-like structures can therefore be manipulated by simply varying pH and temperature in a way that yields the desired actuation. We further demonstrated the potential of as-printed gradient-like structures to function as grippers for grabbing-encapsulating and releasing objects upon thermal or pH stimulation (Figure 5b). Although the surrounding environments may change significantly during the process, the 3D-printed structure before and after the stimulation should be functionally stable. Herein, the three separate synthetic gradient-like structures are stable after long-term use, showing fully repeatable self-bending characteristics (successfully repeated at least 5 times immediately after fabrication, see error bars). Fatigue test were further performed by testing the bending performance after the samples were either stored two weeks in water to maintain the hydration state or exposed to ambient room conditions, confirming that the 3D-printed structures preserved their performance (data included in the error bars) and their structural integrity, *i.e.* without delamination of the individual layers or failure.

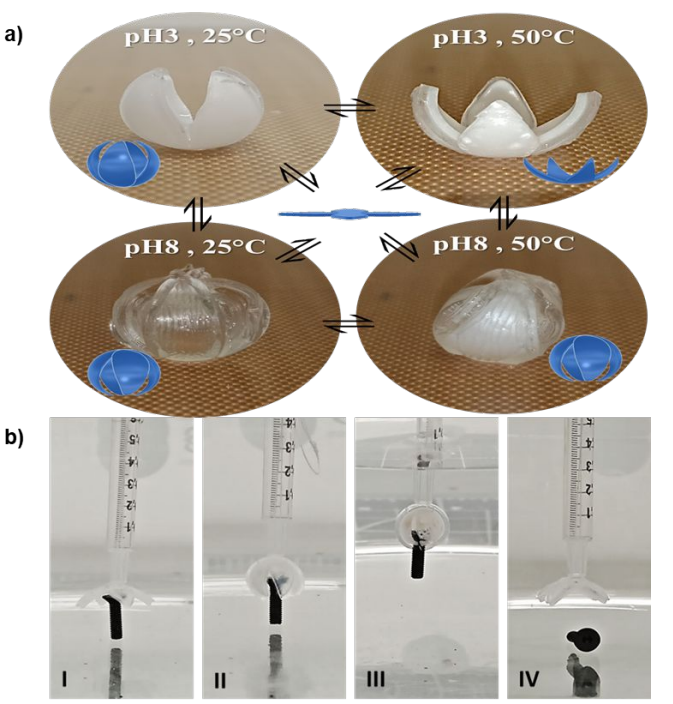

Figure 5. Demonstration of 3D-printed gradient-like structures. (A) temperature and pH dual-responsive actuation of 3D-printed gradient-like structures of varying layer's composition across the hydrogel and **(B)** its use as grippers for grabbing (I-II-III) and releasing (IV) objects upon thermal and pH stimulation.

Conclusions

The present paper aims to mimic biological designs in man-made devices towards designing anisotropy-encoded hydrogel actuators. The latter is achieved from the generation of gradient-like structures where each individual building layers own different volume expansion properties. Fabrication of such gradient-like structures herein relies on the asymmetrical distribution of layer's

surface area to volume ratio, crosslinking density or chemical composition across the hydrogel using the high resolution stereolithography 3D printing. As a result, a family of multi-responsive hydrogel-based actuators with rapid, reversible and repeatable shape-changing characteristics was demonstrated. The bending states of the as-printed structures can be manipulated by simply varying osmotic pressure, temperature and pH in a way that yields the desired actuation. It is the differential swellability of discrete layers within the generated actuators that generates the internal force required to remotely control the material's transformation. Briefly, these three separate synthetic strategies for programming in chemomechanical gradients allow for developing centimeter-scaled actuators capable of *i)* osmotically-driven bending ranging from 0 to 1.4 cm^{-1} in 90s in ethanol and back in 150s in heptane, *ii)* thermally-driven bending ranging from 0 to 1.55 cm^{-1} in 15 min in water at 25°C and back in 15 min in water at 50°C and *iii)* pH-driven bending ranging from 0 to 1.75 cm^{-1} in 45 min at pH 3 and back in 20 min at pH 8 (see Table S1). While the osmotically-driven actuation is limited to one direction, both thermally and pH-driven actuation revealed continuous bidirectional bending. In particular, our work is a platform for designing other 3D-printed hydrogel-based actuators capable of undergoing rapid and controllable motion in response to any immediate environmental change, which offers promise for use in a wide range of technological applications.

Experimental

Materials. *N*-isopropylacrylamide (NIPAM, > 99%, Aldrich), 2-carboxyethylacrylate (CEA, > 99%, Aldrich), *N,N'*-methylenebisacrylamide (MBA, 99 %, Aldrich), diphenyl(2,4,6-trimethylbenzoyl)phosphine oxide (TPO, 97%, Aldrich), hydroquinone (99 %, Aldrich), ethanol (97%, VWR), distilled water and citrate-phosphate buffers were purchased as indicated and used without further purification.

Design and 3D Printing of gradient-like structures. NIPAM and CEA monomers at different ratios together with 1 mol% of MBA crosslinker were dissolved in ethanol to reach a final monomers to ethanol ratio of 1:1. 60 µg of hydroquinone is further included in the formulation as a radical scavenger to improve the resolution of large-scale prints and pot-life of the resins. The final addition of 1 mol% of TPO, a type-I photo-initiator, enables free radical photo-polymerization of the resulting acrylate groups under near-UV exposure. The 3D printer used in this work is an Ember by Autodesk™ desktop controlled by open source software, using a LED projector (λ = 405 nm) with an irradiance of E_e ~ 22.5 $mW.cm^{-2}$. Autodesk Print Studio™ imported, modified and sliced the design into discrete 100 µm layers. The resulting image stack of photo-patterns and the corresponding actions for the 3D printer were exported to a *.tar.gz* file and loaded on to the Ember. Complex 3D-printed gradient-like structures are achieved by controlling either *i)* the feature resolution, *ii)* the dose of UV light and *iii)* the material properties of discrete layers. The latter respectively provide layered structures where *i)* the surface area to volume ratio, *ii)* the crosslinking density and *iii)* the composition of the structure change stepwise along the printing Z-axis. For the hydrogel-based actuators, short layer exposure times (*t* = 2s per 100 µm) yielded high resolution objects. Longer photo-exposures (*t* = 3s and t = 4s per 100 µm) resulted in similar, but stiffer structures consistent with a denser polymer network.

Photo-rheology. We characterized the photo-polymerization reaction using a Discovery Hybrid Rheometer HR-3 (TA Instruments) through constant frequency and amplitude (ϖ = 1 Hz and Γ = 0.5 % strain) oscillatory shear rheology during photo-exposure. We used a circular parallel plate (diameter = 20 mm) with a gap of 1 mm. The fixed bottom plate was transparent acrylic connected to an UV light-source (Omnicure Series 1500, Lumen dynamics) and UV filter (λ = 400-500 nm) using a light guide. A radiometer (Silver Line UV 230-410 nm) placed directly on top of this plate recorded irradiance of E_e = 7.6 $mW{\cdot}cm^{-2}$.

Swelling Ratio Measurements. Swelling of hydrogels are depicted from the equilibrium swelling ratios, kinetics of swelling and kinetics of deswelling[53, 54]. 3D-printed hydrogels in cylindrical shaped (dimensions: 6 mm length, 3 mm thickness) were then soaked in deionized water (starting from the dry state) for the specified time, placed on a dry cellulose pad to remove surface water and then promptly massed. Equilibrium swelling ratios (E) shown in Equation 1 were calculated as the ratio of the mass of a fully swollen hydrogel (W_e, in equilibrium with its medium) to the mass of a dehydrated hydrogel (W_0). Swelling (S) and deswelling (DS) kinetics of hydrogels were interpreted through their mass at predetermined time intervals (W_t) using Equation 2 and Equation 3.

$$E\,(\%) = \frac{W_e - W_0}{W_0} \mathrm{X}\,100 \quad (\mathbf{Eq.\,1})$$

$$S\,(\%) = \frac{W_t - W_0}{W_0} \mathrm{X}\,100 \quad (\mathbf{Eq.\,2})$$

$$DS\,(\%) = \frac{W_e - W_t}{W_e - W_0} \mathrm{X}\,100 \quad (\mathbf{Eq.\,3})$$

We can further determine the nature of diffusion of water into hydrogels by fitting the data to Equation 4 where *F* is the fraction uptake of water ($dw{\cdot}w^{-1}$) at time *t*, *k* is a constant that captures the behavior of the macromolecular network and penetrant, and *n* is the diffusion exponent. Fickian diffusion are defined by the diffusion exponent equal to 0.5. The diffusion coefficients (D) of the cylindrical hydrogels could be estimated from the slope of the *F versus* $t^{1/2}$ curves according to Equation 5.

$$F = \mathrm{k}t^n \quad (\mathbf{Eq.\,4})$$

$$F = 4\left[\frac{Dt}{\pi r^2}\right]^{1/2} \quad (\mathbf{Eq.\,5})$$

Crosslink density determination. The crosslink density (υ_e) of hydrogels can be determined by modulus measurements in the rubbery plateau using Equation 6, where G' is the shear storage modulus in the rubbery plateau (herein taken at a strain of 0.5%), R is the gas constant and T is the temperature in Kelvin corresponding to the storage modulus[50]. Rheological measurements were performed using an Anton Paar Physica Modular Compact Rheometer 501 (MCR-501) to make rough estimate of the effective crosslinking density from the value of elastic moduli. A cone and plate system was used with a 25 mm diameter. Strain sweeps were accordingly performed at a temperature of 25°C and a frequency of 1 Hz from fully swollen samples at a preload of 1N.

$$\upsilon_e = \frac{\mathrm{G}'}{\mathrm{RT}} \quad (\mathbf{Eq.\,6})$$

Actuation. 3D-printed multi-armed grippers swelling reversibly from an initially flat and open state to curved and enclosed within minutes are used to exhibit actuation in response to stimulus. The kinetics of the bending and unbending movements is assessed by plotting the curvature of the object against time (starting from the dry state). From a purely geometric perspective, the bending/unbending curvatures (C) are addressed through the radius (r) of the imaginary circle drown around the actuated object using Equation 7.

$$C = \frac{1}{r} \quad (\mathbf{Eq.\,7})$$

Conflicts of interest

There are no conflicts to declare.

Acknowledgements

We gratefully acknowledge support from the Belgian Federal Government Office of Science Policy (SSTC-PAI 6/27) as well as both Wallonia and the European Commission ''FSE and FEDER". We also acknowledge use of facilities at the Cornell Center for Materials Research (CCMR) supported by the National Science Foundation under Award No. DMR-1120296. J-M. Raquez is a research associate at F.R.S.-FNRS (Belgium).

References

1. A. Sydney Gladman, E. A. Matsumoto, R. G. Nuzzo, L. Mahadevan and J. A. Lewis, *Nat Mater*, 2016, **15**, 413-418.
2. I. Leonid, *Advanced Functional Materials*, 2013, **23**, 4555-4570.
3. S. Armon, E. Efrati, R. Kupferman and E. Sharon, *Science*, 2011, **333**, 1726-1730.
4. Y. Forterre, J. M. Skotheim, J. Dumais and L. Mahadevan, *Nature*, 2005, **433**, 421.
5. J. Knippers, K. G. Nickel and T. Speck, Biomimetic research for architecture and building construction : biological design and integrative structures.
6. W. M. Sokolowski and S. C. Tan, *Journal of Spacecraft and Rockets*, 2007, **44**, 750-754.
7. C. L. Randall, E. Gultepe and D. H. Gracias, *Trends in Biotechnology*, 2012, **30**, 138-146.
8. S. Felton, M. Tolley, E. Demaine, D. Rus and R. Wood, *Science*, 2014, **345**, 644-646.
9. Y. Mao, K. Yu, M. S. Isakov, J. Wu, M. L. Dunn and H. Jerry Qi, *Scientific Reports*, 2015, **5**, 13616.
10. K. Liu, J. Wu, G. H. Paulino and H. J. Qi, *Scientific Reports*, 2017, **7**, 3511.
11. L. Ionov, *Materials Today*, 2014, **17**, 494-503.
12. C. Yao, Z. Liu, C. Yang, W. Wang, X.-J. Ju, R. Xie and L.-Y. Chu, *Advanced Functional Materials*, 2015, **25**, 2980-2991.
13. L. Wang, M. Y. Razzaq, T. Rudolph, M. Heuchel, U. Nöchel, U. Mansfeld, Y. Jiang, O. E. C. Gould, M. Behl, K. Kratz and A. Lendlein, *Materials Horizons*, 2018, DOI: 10.1039/c8mh00266e.
14. H. L. Lim, Y. Hwang, M. Kar and S. Varghese, *Biomaterials Science*, 2014, **2**, 603-618.
15. M. A. C. Stuart, W. T. S. Huck, J. Genzer, M. Müller, C. Ober, M. Stamm, G. B. Sukhorukov, I. Szleifer, V. V. Tsukruk, M. Urban, F. Winnik, S. Zauscher, I. Luzinov and S. Minko, *Nature Materials*, 2010, **9**, 101.
16. L. Ionov, *Journal of Materials Chemistry*, 2010, **20**, 3382-3390.
17. L.-W. Xia, R. Xie, X.-J. Ju, W. Wang, Q. Chen and L.-Y. Chu, *Nature Communications*, 2013, **4**, 2226.
18. L. Ionov, *Soft Matter*, 2011, **7**, 6786-6791.
19. L. Ionov, *Langmuir*, 2015, **31**, 5015-5024.
20. J. Kim, J. A. Hanna, M. Byun, C. D. Santangelo and R. C. Hayward, *Science*, 2012, **335**, 1201-1205.
21. J.-H. Na, N. P. Bende, J. Bae, C. D. Santangelo and R. C. Hayward, *Soft Matter*, 2016, **12**, 4985-4990.
22. Z. L. Wu, M. Moshe, J. Greener, H. Therien-Aubin, Z. Nie, E. Sharon and E. Kumacheva, *Nature Communications*, 2013, **4**, 1586.
23. E. Palleau, D. Morales, M. D. Dickey and O. D. Velev, *Nature Communications*, 2013, **4**, 2257.
24. T.-a. Asoh, M. Matsusaki, T. Kaneko and M. Akashi, *Advanced Materials*, 2008, **20**, 2080-2083.
25. Y. Liu, M. Takafuji, H. Ihara, M. Zhu, M. Yang, K. Gu and W. Guo, *Soft Matter*, 2012, **8**, 3295-3299.
26. X. Li, X. Cai, Y. Gao and M. J. Serpe, *Journal of Materials Chemistry B*, 2017, **5**, 2804-2812.
27. L. Wang, Y. Jian, X. Le, W. Lu, C. Ma, J. Zhang, Y. Huang, C.-F. Huang and T. Chen, *Chem. Commun.*, 2018, **54**, 1229-1232.
28. J. Zheng, P. Xiao, X. Le, W. Lu, P. Théato, C. Ma, B. Du, J. Zhang, Y. Huang and T. Chen, *Journal of Materials Chemistry C*, 2018, **6**, 1320-1327.
29. C. Ma, W. Lu, X. Yang, J. He, X. Le, L. Wang, J. Zhang, M. J. Serpe, Y. Huang and T. Chen, *Advanced Functional Materials*, 2018, **28**, 1704568.
30. D. Morales, I. Podolsky, R. Mailen, T. Shay, M. Dickey and O. Velev, *Micromachines*, 2016, **7**, 98.
31. C. K. Chua and K. F. Leong, *3D Printing and Additive Manufacturing: Principles and Applications*, World Scientific, 5th edn., 2015.
32. L. Gibson, D. Rosen and B. Stucker, *additive manufacturing technologies: 3D Printing, Rapid Prototyping, and Direct Digital Manufacturing*, Springer, 2015.
33. F. Momeni, S. M.Mehdi Hassani.N, X. Liu and J. Ni, *Materials & Design*, 2017, **122**, 42-79.
34. E. Pei and G. H. Loh, *Progress in Additive Manufacturing*, 2018, **3**, 95-107.
35. S. Miao, N. Castro, M. Nowicki, L. Xia, H. Cui, X. Zhou, W. Zhu, S.-j. Lee, K. Sarkar, G. Vozzi, Y. Tabata, J. Fisher and L. G. Zhang, *Materials Today*, 2017, **20**, 577-591.
36. S. Tibbits, *Architectural Design*, 2014, **84**, 116-121.
37. D. Raviv, W. Zhao, C. McKnelly, A. Papadopoulou, A. Kadambi, B. Shi, S. Hirsch, D. Dikovsky, M. Zyracki, C. Olguin, R. Raskar and S. Tibbits, *Scientific Reports*, 2014, **4**, 7422.
38. N. Oxman, *Virtual and Physical Prototyping*, 2011, **6**, 3-31.
39. N. Oxman, E. Tsai and M. Firstenberg, *Virtual and Physical Prototyping*, 2012, **7**, 261-274.
40. K. U. Claussen, T. Scheibel, H.-W. Schmidt and R. Giesa, *Macromol. Mater. Eng.*, 2012, **297**, 938-957.
41. M. Naebe and K. Shirvanimoghaddam, *Applied Materials Today*, 2016, **5**, 223-245.
42. T. J. Wallin, J. Pikul and R. F. Shepherd, *Nature Reviews Materials*, 2018, **3**, 84-100.
43. J.-W. Choi, H.-C. Kim and R. Wicker, *Journal of Materials Processing Technology*, 2011, **211**, 318-328.
44. R. B. Wicker and E. W. MacDonald, *Virtual and Physical Prototyping*, 2012, **7**, 181-194.
45. E. Sinibaldi, A. Argiolas, G. L. Puleo and B. Mazzolai, *PLOS ONE*, 2014, **9**, e102461.
46. T. Tanaka and D. J. Fillmore, *The Journal of Chemical Physics*, 1979, **70**, 1214-1218.
47. Q. Zhao, J. W. C. Dunlop, X. Qiu, F. Huang, Z. Zhang, J. Heyda, J. Dzubiella, M. Antonietti and J. Yuan, *Nature Communications*, 2014, **5**, 4293.

48. H. Yuk, S. Lin, C. Ma, M. Takaffoli, N. X. Fang and X. Zhao, *Nature Communications*, 2017, **8**, 14230.
49. D. Roy, W. L. A. Brooks and B. S. Sumerlin, *Chemical Society Reviews*, 2013, **42**, 7214-7243.
50. L. W. Hill, *Progress in Organic Coatings*, 1997, **31**, 235-243.
51. M. Rizwan, R. Yahya, A. Hassan, M. Yar, A. Azzahari, V. Selvanathan, F. Sonsudin and C. Abouloula, *Polymers*, 2017, **9**, 137.
52. Y. Pei, J. Chen, L. Yang, L. Shi, Q. Tao, B. Hui and J. Li, *Journal of Biomaterials Science, Polymer Edition*, 2004, **15**, 585-594.
53. S. Petrusic, M. Lewandowski, S. Giraud, P. Jovancic, B. Bugarski, S. Ostojic and V. Koncar, *J. Appl. Polym. Sci.*, 2012, **124**, 890-903.
54. D. Saraydin, E. Karadağ and O. Guven, *Polym J*, 1997, **29**, 631-636.